Chemistry
A European
Journal

Chemistry Europe
European Chemical Societies Publishing

Accepted Article

Title: Computational and Experimental Study of Turbo-Organomagnesium Amide Reagents: Cubane Aggregates as Reactive Intermediates in Pummerer Coupling

Authors: Ferran Planas, Stefanie V. Kohlhepp, Genping Huang, Abraham Mendoza, and Fahmi Himo

To be cited as: *Chem. Eur. J.* 10.1002/chem.202004164

Link to VoR: https://doi.org/10.1002/chem.202004164

WILEY-VCH

10.1002/chem.202004164

Computational and Experimental Study of Turbo-Organomagnesium Amide Reagents: Cubane Aggregates as Reactive Intermediates in Pummerer Coupling

Ferran Planas,[†] Stefanie V. Kohlhepp,[†] Genping Huang,[§] Abraham Mendoza,[†]* and Fahmi Himo[†]*

[†] Department of Organic Chemistry, Arrhenius Laboratory, Stockholm University, SE-106 91 Stockholm, Sweden

[§] Department of Chemistry, School of Science, Tianjin University, Tianjin 300072, P. R. China

Corresponding authors: Fahmi.Himo@su.se , Abraham.Mendoza@su.se

Abstract

The dynamic equilibria of organomagnesium reagents are known to be very complex, and the relative reactivity of their components is poorly understood. Herein, a combination of DFT calculations and kinetic experiments is employed to investigate the detailed reaction mechanism of the Pummerer coupling between sulfoxides and turbo-organomagnesium amides. Among the various aggregates studied, unprecedented heterometallic open cubane structures are demonstrated to yield favorable barriers through a concerted anion-anion coupling / S–O cleavage step. Beyond a structural curiosity, these results introduce open cubane organometallics as key reactive intermediates in turbo-organomagnesium amide mixtures.

Introduction

Main group organometallics are the most common source of nucleophilic carbon in organic synthesis. Grignard reagents (R-MgX; **1**) have been particularly instrumental due to their balanced reactivity, cost, and functional group tolerance.[1] Structural studies in the solid-state and solution dynamics of these seemingly simple organometallics have demonstrated the complexity of their aggregation equilibria, often involving various species co-existing in solution (Scheme 1A).[2,3] The Schlenk-equilibrium yields diorganomagnesium species **2** and it is an important example of this dynamic behavior, which is influenced by concentration, solvent, steric properties of the carbon fragment, halide anion, and temperature.[4,5] The presence of magnesium or lithium salts fundamentally changes the reactivity of Grignard reagents and affects the positions of these equilibria through the formation of mono- or multinuclear complexes with variable relative stabilities and reactivities (*i.e.* "linear" dimers **1a**, LiCl adducts **1b**, "ate" complexes **1c**, open cubane aggregates **1d**, etc.).[3,6] Despite the studies on the solution equilibria of these systems to determine the most abundant species in different conditions, their relative contributions to the overall reactivity is difficult to assess. This is due to the problematic deconvolution of the roles that various aggregates take in the overall kinetic progress of the reaction.

The solution equilibria of magnesium amide bases (R_2N–MgX), termed 'Hauser' bases **3** (Scheme 1B),[7] and their LiCl complexes, known as 'Knochel-Hauser' or '*turbo*-Hauser' bases **4**, are governed by similar principles.[8,9] These reagents have been mostly used in the selective magnesiation of C–H bonds.[10] They are structurally diverse and the amide ligand can occupy bridging or terminal positions.[8,9,11-13] Hauser bases have been combined with Grignard reagents to drive the most challenging deprotonations. The resulting organomagnesium amides (**5**; R–Mg–NR_2) turn the acid-base reaction irreversible through deprotonation of the initially formed amine with the magnesium alkyl.[14] The solution dynamics of these reagents are significantly more complex than their parent components. The Schlenk (diorganomagnesium and magnesium halide clusters) and aggregation (monomeric, dimeric, etc.) equilibria on the Grignard and Hauser base co-exist with various heteroleptic organomagnesium amide complexes. Understandably, the structural information on these systems is limited to solid-state studies, in which dimeric structures with bridging amide ligands are most common (see **5**, Scheme 1A).[15]

10.1002/chem.202004164

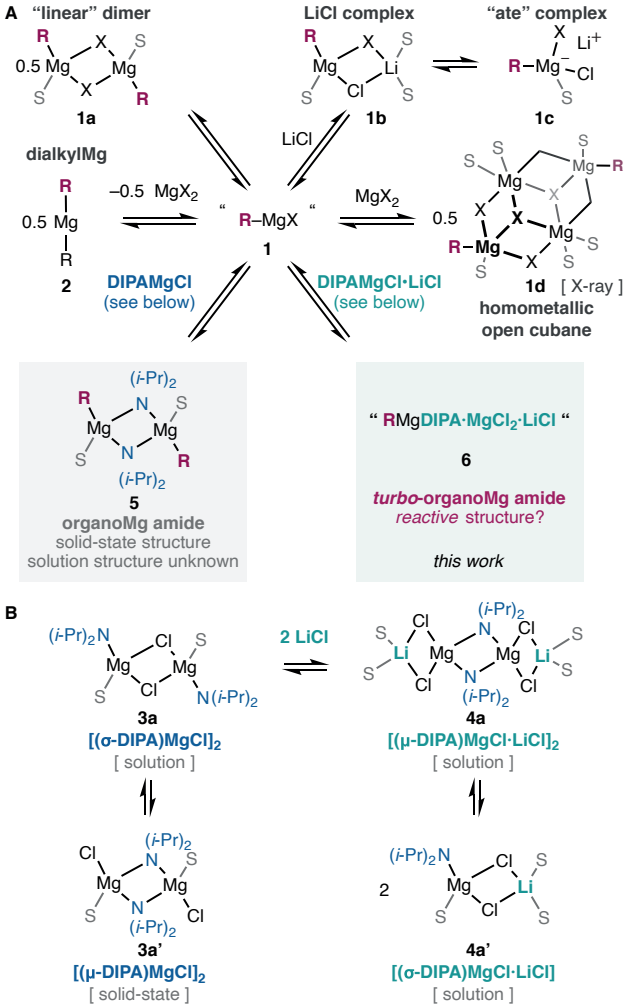

Scheme 1. *Relevant structures involved in the solution equilibria of Grignard reagents and their organomagnesium amides (A), or Hauser and Knochel-Hauser bases (B). For simplicity, only the most common dominant species are shown. DIPA, diisopropylamide; S, solvent.*

Recently, Mendoza and co-workers discovered the differential reactivity of Grignard reagents **1** upon the addition of a specific Knochel-Hauser base (DIPAMgCl·LiCl; **4a**) in the context of Pummerer-type reactions (Scheme 2A).[16] This process allows the direct transformation of sulfoxides **7** into α-functionalized sulfides **8**. Unlike conventional electrophilic Pummerer reactions, this method is compatible with strong and localized alkyl-, aryl-, vinyl- and alkynyl-Grignard nucleophiles. This work introduced the potential of *turbo*-magnesium amides as activators of organometallics, beyond their role as bases in earlier work.[10,14] Surprisingly, the mixture of Grignard **1** and DIPAMgCl·LiCl (**4a**) eluded the fast S-Mg exchange that occurs between Grignards **1** and sulfoxides **7** at cryogenic temperatures.[17] Interestingly, control experiments without **4a** (entries 1 and 2; Scheme 2A) or with a similar Knochel-Hauser base **4b** (entry 3) clearly indicated the importance of the diisopropylamide

fragment,[8] which pointed to a critical aggregation of Grignard **1** with the base **4a** into a new *turbo*-organomagnesium amide species **6**. It was also found that LiCl (entry 4), and in particular the 1:1:1 stoichiometry between the Grignard, the base and LiCl, are critical for the success of this reaction (entries 5 and 6). Moreover, it was recently found that the same Grignard-DIPAMgCl·LiCl combination is uniquely more reactive and more selective in addition reactions to challenging carboxylate anions.[18] This further suggests that a new species is formed in solution upon mixing Grignard reagents **1** and DIPAMgCl·LiCl (**4a**), and this is relevant for the new reactivity observed.

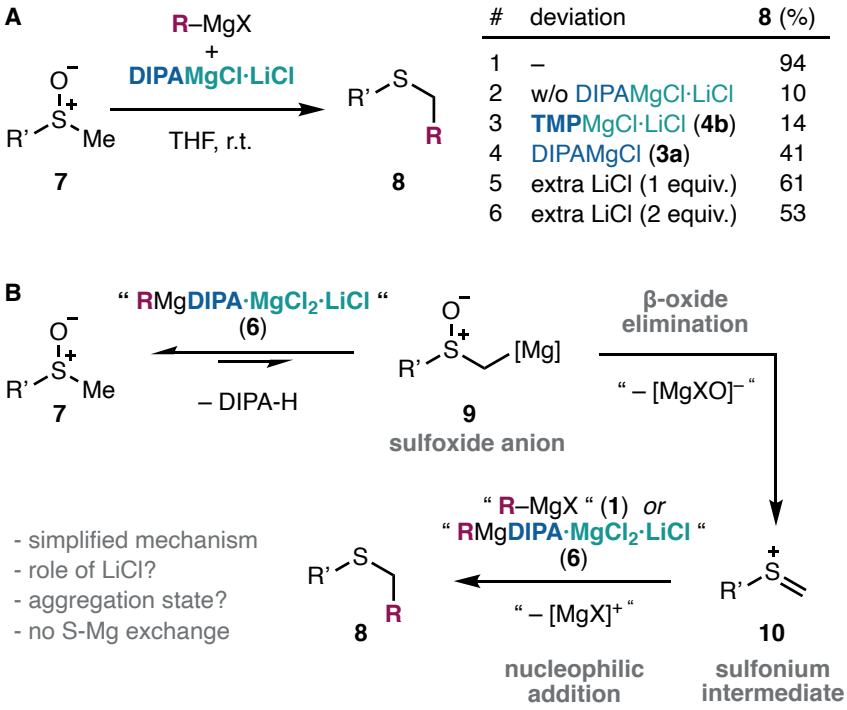

Scheme 2. *(A) Pummerer coupling between sulfoxides and Grignard reagents* ***1*** *mediated by the turbo-Hauser base DIPAMgCl·LiCl (****4a****) including key optimization studies.[16] (B) Previous mechanistic proposal.*

Although the exact mechanism of the Grignard activation by DIPAMgCl·LiCl (**4a**) in this process was unclear, the initially proposed mechanism was consistent with previous knowledge on related β-functionalized organolithiums[19] and Pummerer reactions (Scheme 2B).[20] The deprotonation of the sulfoxide **7** would produce a sulfoxide anion **9**, which would undergo S–O bond excision through β-oxide elimination[19] to generate a Pummerer sulfonium intermediate **10**.[20] The latter would react with an undefined nucleophilic Grignard species **1,6** to generate the thioether product **8**.

To gain insight into the intimate mechanism of activation of the Grignard reagent **1** bestowed by the Knochel-Hauser base **4a**, we set out to undertake a computational and kinetic profiling of this system. At the onset, it is important to underscore that only solid-state information existed on some organomagnesium amides **5**[15] and none on the LiCl adducts **6** that seemed to be responsible for the differential reactivity observed (see Scheme 2A). Given the complex equilibria that may be at place in solutions of *turbo*-organomagnesium amides **6**, the combined experimental-computational approach allows to evaluate the energies of various aggregates, as well as their relative relevance for the reactivity towards sulfoxides **7**.

Results and Discussion

In both the experimental and computational investigations described below, the reaction was studied using methyl phenyl sulfoxide (**7a**) and isopropylmagnesium chloride (**1e**) as representative reactants.

First, we set out to observe the evolution of the system using *in situ* no-D ^{1}H-NMR spectroscopy. The sulfoxide **7a** displayed broadened and shifted resonances when the base DIPAMgCl·LiCl **4a** and Grignard **1e** were subsequently added, thus suggesting interaction through several complexes in equilibrium (see SI). This mixture is unstable and evolves into the product even at low temperature, thus preventing structural studies on this equilibrium by NMR or XRD. As discussed above, the dominant structures participating in this rapid equilibrium may not be relevant for the reactivity, and the reactive species may be minor components. The formation of the product could be monitored by NMR, finding that the reaction reached 91% yield in about 3h at 25°C (Scheme 3).

Next, we employed density functional theory (DFT) calculations, in the form of the dispersion-corrected B3LYP method,[21,22] to determine the structures of the most stable species that can form initially under the experimental conditions. To that end, we optimized the structures of various aggregates that can form prior to the addition of the sulfoxide, and compared their energies to those of the monomer of the magnesium amide and the dimer of the Grignard reagent, as these two have been reported to be dominant forms of the respective reagents in solution.[8,4b] This study concluded that the aggregation of the Grignard reagent and DIPAMgCl·LiCl results in more stable heteroleptic aggregates (see SI for details).

The two most stable complexes with linear topology and two open cubane complexes were then used to explore the coordination of the sulfoxide substrate. In all cases, the exchange of one solvent molecule for the sulfoxide at the terminal magnesium resulted in complexes that

10.1002/chem.202004164

are 3-6 kcal/mol more stable (see SI). The exothermic character of this ligand substitution is consistent with the interaction observed by ^{1}H-NMR in the reaction mixture (see above). The resulting complexes **A-D** are shown in Figure 1 along with their calculated relative energies.

Complex **A** consists of two magnesium ions bridged by the amide and a chloride ion. One magnesium ion binds the sulfoxide and the isopropyl moiety, while the other ion binds a second chloride and a THF molecule. Complex **B** is essentially the lithium chloride adduct of complex **A**, where two chlorides bridge the Mg and the Li ions. This structural motif is commonly found in related Grignard and Hauser-base complexes.[8-10,12] The energy of complex **B** is only 0.2 kcal/mol higher than complex **A**.

Despite not being reported in structural studies, we explored the feasibility of the magnesium-lithium heterometallic open cubanes **C** and **D** as reactive intermediates. Similar cubane and open cubane structures have been implicated in unrelated reactions involving potassium[23] or zinc aggregates.[24] Complex **C** features two magnesium ions linked by the amide and a chloride, with additional chloride bridges with the lithium ion to complete the compact structure. This species is calculated to be +3.3 kcal/mol relative to complex **A**. Complex **D** is a dimer formed of two units of complex **C**. This aggregate is calculated to be only 4.4 kcal/mol higher than complex **A**. As seen in Figure 1, in complexes **A-D** the amide bridges two magnesium ions while the sulfoxide and alkyl ligand bind to a single magnesium. Exchanging of the positions of the amide and sulfoxide leads to higher energies (see SI).

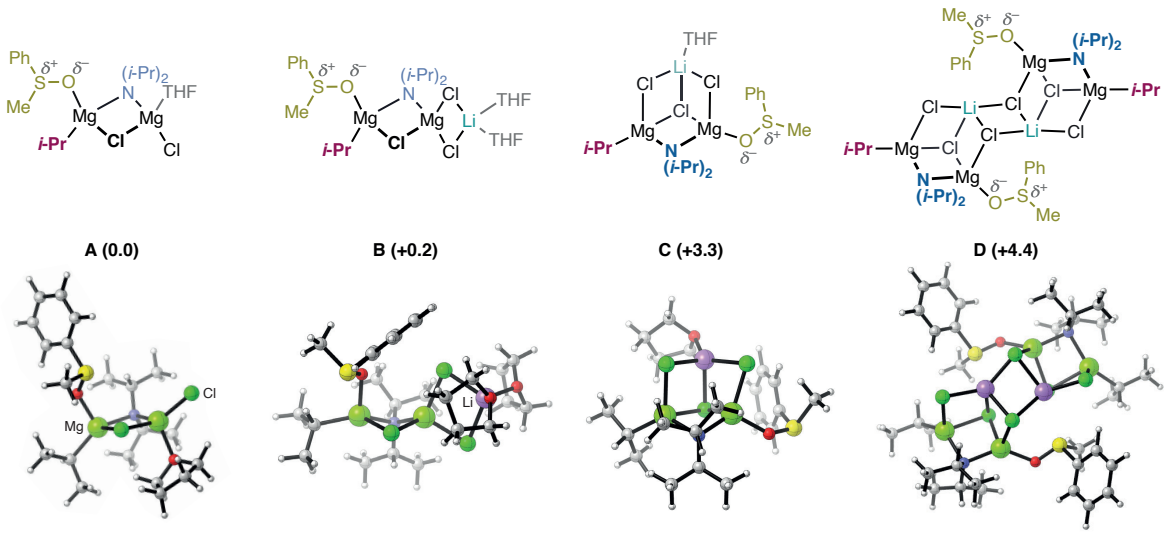

Figure 1. *Structures of the four starting complexes used to study the reaction mechanism. Relative energies are indicated in kcal/mol. For important distances in these structures, see SI.*

10.1002/chem.202004164

Next, we calculated the full reaction mechanisms starting from these four complexes. The calculations show that they follow essentially the same reaction mechanism, consisting of the following steps: 1) a ligand rearrangement into a μ-sulfoxide / σ-amide disposition, 2) a proton transfer from the sulfoxide α-carbon to the amide, forming a sulfoxide enolate featuring an S=C double bond, and finally 3) a nucleophilic addition of the isopropyl moiety to the sp^2 carbon of the sulfoxide anion taking place concertedly with the cleavage of the S–O bond. The latter of these steps is a surprising anion-anion C–C coupling that contrasts with electrophilic Pummerer reactions via sulfonium intermediates **10**.[20]

As shown in Figure 2, the calculations demonstrate that the two linear complexes **A** and **B** have very similar reaction energy profiles. The optimized geometries of the intermediates and transition states (TSs) for both complexes are given in the SI. The last step was found to be rate-determining for both cases, with a calculated barrier of 27.1 kcal/mol for complex **A** and 28.1 kcal/mol for complex **B**. An important observation here is that, in contrast to previous proposals,[16a] the β-oxide elimination pathway[19] to form a discrete sulfonium intermediate[20] could not be obtained by the calculations (see SI for details).

The overall barriers calculated for these two complexes are not compatible with the reaction time and temperature used in the experiments, indicating that the two considered linear complexes might not be the active species in the reaction. Furthermore, the fact that identical mechanisms were obtained for complexes **A** and **B**, with very similar barriers, suggests that other linear complexes (*e.g.* complexes **E**-**K** in the Supporting Information) are also likely to behave similarly, yielding high barriers. These complexes were therefore not considered further by the calculations.

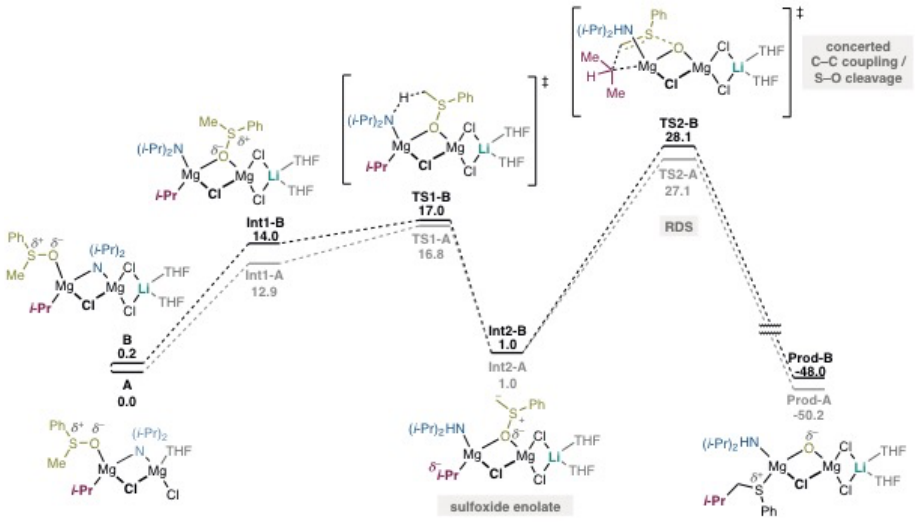

Figure 2. *Free-energy profile of the reaction mechanism of complexes **A** and **B**. Relative energies are in kcal/mol.*

10.1002/chem.202004164

We then turned our attention to reactions starting from the open cubane structures **C** and **D**. These two complexes gave similar energy profiles compared to each other, but very different compared to the linear structures discussed above. The calculated energy graph and the optimized geometries of the intermediates and transition states for the reaction starting from complex **C** are depicted in Figures 3 and 4, while the corresponding figures for complex **D** are given in the SI.

According to this mechanism, the first step also here is the formation of the intermediate with the sulfoxide in the bridging position and the amide in the terminal one (σ-amide; **Int1-C**). The energy of this intermediate is 7.7 kcal/mol higher than complex **C**, i.e. +11.0 kcal/mol compared to the most stable complex **A**. This rearrangement is necessary, as the direct deprotonation of the sulfoxide in the terminal position is associated with high barriers (see SI), probably due to the coordinative saturation of the bridged amide (μ-amide) that prevents the proton abstraction. Next, **Int1-C** undergoes a second rearrangement step to form **Int2-C**, 2.2 kcal/mol higher in energy, in which the oxygen of the sulfoxide is bound to the three metallic ions (see Figures 3 and 4). **Int2-C** can then undergo the intramolecular proton transfer through **TS1-C**, which has an accumulated barrier of 16.8 kcal/mol relative to complex **C**, i.e. 20.1 kcal/mol relative to the most stable species, complex **A**. Interestingly, in the resulting **Int3-C** (Figure 4), the anionic carbon of the sulfoxide enolate binds to the Mg ion (Mg–C distance 2.22 Å), displacing the oxygen, which is no longer bridging (Mg–O distance 2.66 Å). At **Int2-C**, the alternative proton transfer to the isopropyl moiety has a more than 11 kcal/mol higher barrier compared to **TS1-C** and can be ruled out (see SI).

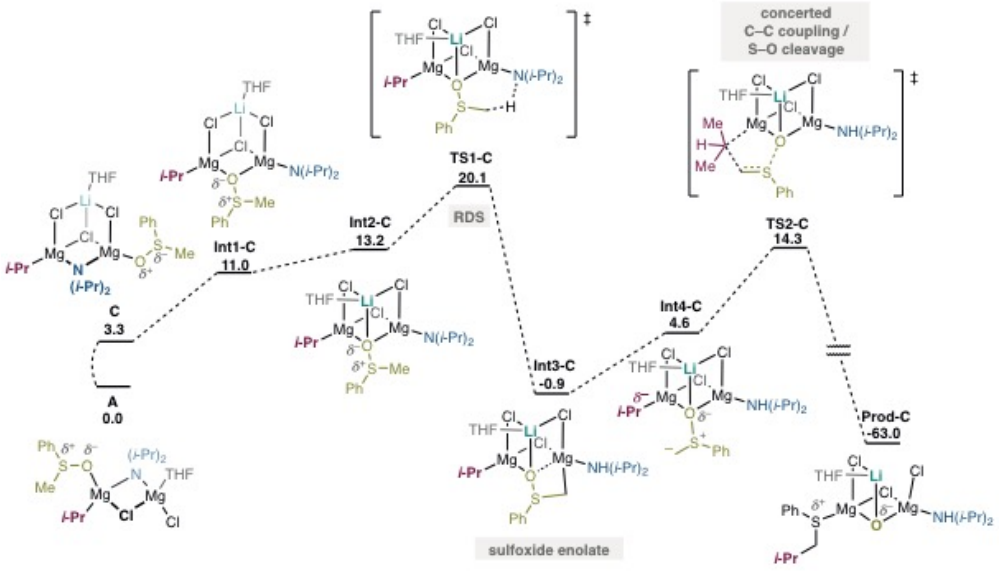

Figure 3. *Free-energy profile of the reaction mechanism of complex **C**. Relative energies are in kcal/mol.*

Int3-C is calculated to be 14.1 kcal/mol lower than **Int2-C** (-0.9 kcal/mol relative to complex **A**), and in order for the reaction to proceed, another rearrangement step is necessary, namely the sulfoxide rotates around the S–O bond to form **Int4-C**, which is calculated to be 5.5 kcal/mol higher than **Int3-C**. This rotation breaks the Mg–C coordination, resulting in an sp^2-hybridized anion in close proximity with the isopropyl moiety (**Int4-C**). In the final step of the reaction, the isopropyl adds to the sulfoxide enolate concertedly with the cleavage of the S–O bond to form the final product, similarly to the mechanism found for the linear complexes **A** and **B**. The cumulative barrier for this step is calculated to be 15.2 kcal/mol relative to **Int3-C** (see Figure 3). In the transition state for the C–C bond formation (**TS2-C**), the Li–O distance is 1.82 Å, which is 0.17 Å shorter than in the preceding intermediate due to the increasing negative charge on the oxygen. This shorter distance, in turn, increases the congestion in the complex, which results in the chloride that is bridging the Li and Mg ions becoming terminal.

The rate-determining barrier of this mechanism is thus 20.1 kcal/mol, which is 7-8 kcal/mol lower than the barriers obtained for the linear complexes **A** and **B**. Interestingly, the energies for the reaction starting from the double cubane complex **D** are similar to those of complex **C** (details given in SI), with a calculated rate-determining barrier of 24.9 kcal/mol. Hence, despite the fact that the cubane starting structures are slightly higher in energy compared to the linear ones (Figure 1), they lead to reaction mechanisms with lower barriers. One reason is the greater extent of electrostatic stabilization of the negative charge of the oxygen upon cleavage of the S–O bond due to the complexation of the lithium ion. This stabilization can be detected from the shortening of the Li–O distance at the last step, and also from the much lower energy of the final product, which is calculated to be much more stable than the products of the linear complexes (compare, for example, **Prod-C** in Figure 3 with **Prod-A** in Figure 2).

It is also interesting to note that the S–O bond distance of the sulfoxide enolate of **Int4-C** is 0.10 Å longer than the corresponding distance for complex **B**. Moreover, the sp^2 carbon in **Int4-C** has less negative charge (–0.82) compared to the corresponding intermediate for complex **B** (–0.97), indicating that the carbon in **Int4-C** would facilitate coupling with the alkyl nucleophile in the case of the open cubane structure (see SI for details).

10.1002/chem.202004164

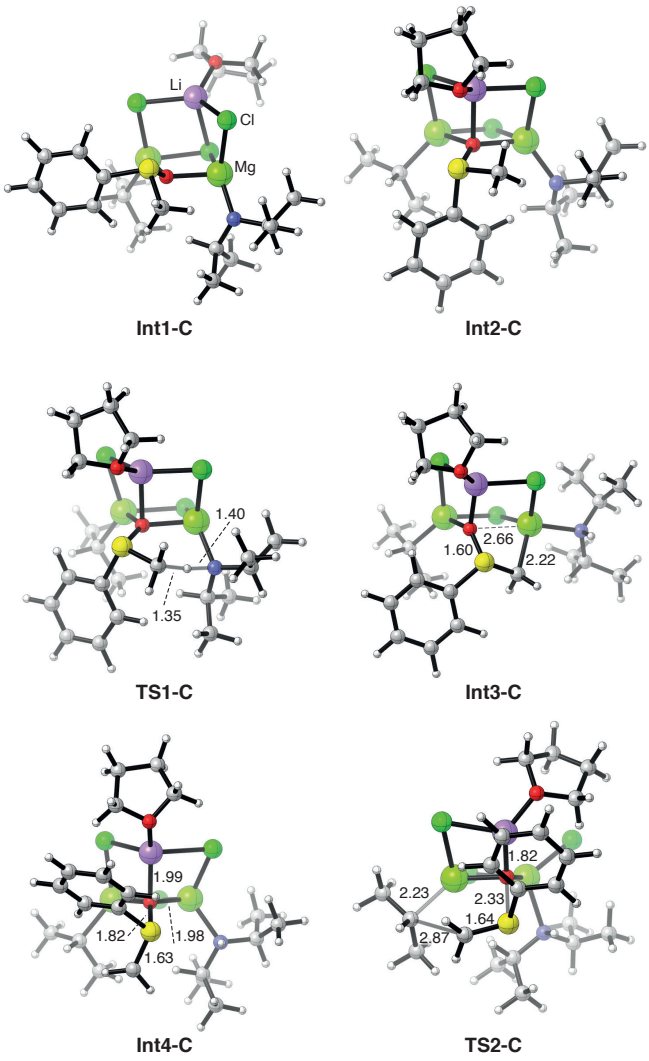

***Figure 4**. Optimized geometries of the intermediates and transition states of the reaction mechanism for complex **C**. Selected distances are given in Angstrom.*

An important difference between the reactions of the linear complexes and the cubane ones is that the C–C bond formation is rate-limiting in the former, while in the latter the proton transfer step is rate-limiting. The fact that this step is also irreversible implies that one would expect to observe a primary kinetic isotope effect (KIE) when using an analogous deuterated substrate if the predictions of the calculations are correct. Indeed, we observed a significantly slower reaction using sulfoxide **7a-*d*$_3$**, reaching only 48% yield in the first 3.3 hours as evidenced by ^{1}H-NMR (Scheme 3). This contrasts with the complete conversion in the same time obtained with the protonated substrate **7a**. However, the complex kinetics observed in the system prevented an accurate determination of the KIE value. The deprotonation equilibrium could also affect the KIE observed, but the irreversible deprotonation predicted by the calculations makes this scenario less likely. The mechanism involving chiral cubane

intermediates presented herein may also explain the partial chirality transfer observed for more complex substrates,[16a] which was initially ascribed to an intimate sulfonium ion pair in line with earlier Pummerer literature.

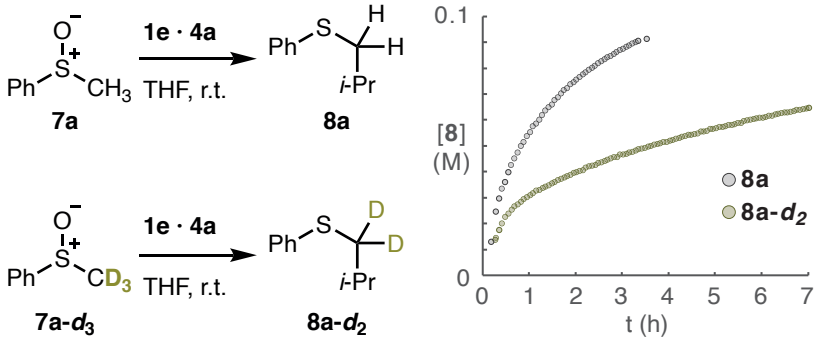

***Scheme 3**. The slower reaction with a deuterated substrate **7a-d₃** is consistent with the rate-determining deprotonation predicted by the calculations.*

Conclusions

In summary, the Pummerer reaction between sulfoxides and Grignard nucleophiles activated by *turbo*-Hauser bases has been calculated to occur through an open-cubane heterometallic *turbo*-organomagnesium amide. The caged topology of this intermediate is crucial to facilitate the activation of the S–O bond and stabilize the negative charge on the sulfoxide enolate carbon. Surprisingly, the formation of the new C–C bond occurs through a concerted anion-anion coupling with concomitant cleavage of the S–O bond. This contrasts with conventional Pummerer-type reactions operating through electrophilic intermediates. These insights explain the critical role of LiCl in nucleophilic Pummerer coupling, and open new avenues for research in new synthetic methods based on the synergy between Knochel-Hauser bases and Grignard reagents.

Computational Methods

All the calculations were performed with the package Gaussian 09[25] and the B3LYP-D3(BJ) functional.[21,22] Geometry optimizations and frequency calculations were carried out with the 6-31G(*d,p*) basis set. Solvation effects were considered by performing single-point calculations with the SMD model and THF as solvent.[26] To obtain better accuracy, the electronic energies of the optimized structures were calculated using single-point calculations with the larger basis set 6-311+G(2*d,2p*). Vibrational frequencies were calculated at the same level of theory as the

geometry optimization, and the Gibbs free energy corrections were calculated using the rigid-rotor-harmonic-oscillator (RRHO) approximation at room temperature. Standard state corrections to account for the conversion from the 1 atm ideal gas to the 1 M standard state for the solutes and the 12.3 M for the solvent were included. This correction was done by adding the term RT ln(24.5) = +1.9 kcal/mol for the solutes and RT ln(24.5·12.3) = +3.4 kcal/mol for the solvent.

Supporting Information

Further computational results, absolute energies and energy corrections, and Cartesian coordinates of reported structures (PDF). Experimental procedures, kinetic monitoring and data analysis (PDF).

Acknowledgements

FH thanks the Swedish Research Council for financial support. AM thanks the Knut and Alice Wallenberg Foundation (KAW2016.0153) and the European Research Council (714737) for financial support.

References

1. (a) Knochel, P. In Organometallics in Synthesis: Organomagnesium and Organozinc Chemistry: Wiley, VCH; **2013**. (b) Knochel, P.; Kmsovskiy, A.; Sapountzis, L. In Handbook of Functionalized Organometallics: Applications in Synthesis. Weinheim: Wiley-VCH; **2008** (c) Knochel, P.; Dohle, W.; Gommermann, N.; Kneisel, F. F.; Kopp, F.; Korn, T.; Sapountzis, I.; Vu, V. A. Highly Functionalized Organomagnesium Reagents Prepared through Halogen-Metal Exchange. *Angew. Chem., Int. Ed.* **2003**, *42*, 4302–4320.; For an account on the use of Grignard reagents in process scale, see: (d) Tilstam, U.; Weinmann, H. Activation of Mg Metal for Safe Formation of Grignard Reagents on Plant Scale. *Org. Proc. Res. Dev.* **2002**, *6*, 906–910.

2. (a) For an NMR solution study on Grignard and turbo-Grignard reagents, see: Schnegelsberg, C.; Bachmann, S.; Kolter, M.; Auth, T.; John, M.; Stalke, D.; Koszinowski, K. Association and Dissociation of Grignard Reagents RMgCl and Their Turbo Variant RMgCl·LiCl. *Chem. - Eur. J.* **2016**, *22*, 7752–7762.; (b) For an X-ray and CSI-MS study on Grignard reagents, see: Sakamoto, S.; Imamoto, T.; Yamaguchi, K. Constitution of Grignard

Reagent RMgCl in Tetrahydrofuran. *Org. Lett.* **2001**, *3*, 1793–1795.

3. Peltzer, R. M.; Gauss, J.; Eisenstein, O.; Cascella, M. The Grignard Reaction – Unraveling a Chemical Puzzle. *J. Am. Chem. Soc*. **2020**, *142*, 2984-2994.

4. (a) Seyferth, D. The Grignard Reagents. *Organometallics*. **2009**, *28*, 1598–1605.; (b) For a recent computational study, see: Peltzer, R. M.; Eisenstein, O.; Nova, A.; Cascella, M. How Solvent Dynamics Controls the Schlenk Equilibrium of Grignard Reagents: A Computational Study of CH_3MgCl in Tetrahydrofuran. *J. Phys. Chem. B.* **2017**, *121*, 4226-4237.

5. For a comprehensive structural review, see: Harrison-Marchand, A.; Mongin, F. Mixed AggregAte (MAA): A Single Concept for All Dipolar Organometallic Aggregates. 1. *Structural Data. Chem. Rev.* **2013**, *113*, 7470-7562.

6. (a) Krasovskiy, A.; Knochel, P., A LiCl-Mediated Br/Mg Exchange Reaction for the Preparation of Functionalized Aryl- and Heteroarylmagnesium Compounds from Organic Bromides. *Angew. Chem., Int. Ed*. **2004**, *43*, 3333-3336.; (b) Knochel, P.; M. Barl, N.; Werner, V.; Sämann, C., The Halogen/Magnesium-Exchange Using *i*-PrMgCl·LiCl and Related Exchange Reagents. *Heterocycles.* **2014**, *88*, 827-844.

7. (a) Hauser, C. R.; Walker, H. G. Condensation of Certain Esters by Means of Diethylaminomagnesium Bromide. *J. Am. Chem. Soc.* **1947**, *69*, 295–297; Eaton introduced DIPA and TMP as hindered magnesium bases: (b) Eaton, P. E.; Lee, C. H.; Xiong, Y. Magnesium Amide Bases and Amido-Grignards. 1. Ortho Magnesiation. *J. Am. Chem. Soc.* **1989**, *111*, 8016–8018.

8. Neufeld, R.; Teuteberg, T. L.; Herbst-Irmer, R.; Mata, R. A.; Stalke, D. Solution Structures of Hauser Base $^{i}Pr_2NMgCl$ and Turbo-Hauser Base $^{i}Pr_2NMgCl·LiCl$ in THF and the Influence of LiCl on the Schlenk-Equilibrium. *J. Am. Chem. Soc.* **2016**, *138*, 4796–4806.; (b) Neufeld, R.; Stalke, D., Solution Structure of Turbo-Hauser Base TMPMgCl · LiCl in [D8]THF. *Chem. Eur. J.* **2016**, *22*, 12624-12628; (c) Armstrong, D. R.; García-Álvarez, P.; Kennedy, A. R.; Mulvey, R. E.; Parkinson, J. A. Diisopropylamide and TMP Turbo-Grignard Reagents: A Structural Rationale for their Contrasting Reactivities. *Angew. Chem., Int. Ed*. **2010**, *49*, 3185−3188.

9. For the solid-state structure of TMPMgCl·LiCl, see: (a) García-Álvarez, P.; Graham, D. V.; Hevia, E.; Kennedy, A. R.; Klett, J.; Mulvey, R. E.; O'Hara, C. T.; Weatherstone, S. Unmasking Representative Structures of TMP-Active Hauser and Turbo-Hauser Bases. *Angew. Chem., Int. Ed.* **2008**, *47*, 8079–8081.; For the solid-state structure of DIPAMgCl·LiCl, see ref. 8c.

10. (a) Melzig, L.; Rauhut, C. B.; Knochel, P. 2,3-Functionalization of Furans, Benzofurans and Thiophenes via Magnesiation and Sulfoxide-Magnesium Exchange. *Chem. Commun.* **2009**, *24*, 3536–3538.; (b) Rohbogner, C. J.; Wunderlich, S. H.; Clososki, G. C.; Knochel, P. New Mixed Li/Mg and Li/Mg/Zn Amides for the Chemoselective Metallation of Arenes and Heteroarenes. *Eur. J. Org. Chem.* **2009**, *11*, 1781–1795.; (c) Clososki, G. C.; Rohbogner, C. J.; Knochel, P. Direct Magnesiation of Polyfunctionalized Arenes and Heteroarenes Using $(Tmp)_2Mg \cdot 2\,LiCl$. *Angew. Chem., Int. Ed.* **2007**, *46*, 7681–7684.; (d) Krasovskiy, A.; Krasovskaya, V.; Knochel, P. Mixed Mg/Li Amides of the Type $R_2NMgCl \cdot LiCl$ as Highly Efficient Bases for the Regioselective Generation of Functionalized Aryl and Heteroaryl Magnesium Compounds. *Angew. Chem., Int. Ed.* **2006**, *45*, 2958–2961.

11. Hauser-bases like DIPAMgCl are mostly dimeric species that display bridging amido ligands in the solid-state. However, they have been shown to be likely chloro-bridged in solution, thus illustrating the small energetic difference between these coordination manifolds (see ref. 8)

12. The Knochel-Hauser bases DIPAMgCl.LiCl is dimeric in the solid state with bridging amide ligands, but equilibrates with its monomer in solution (see ref. 8).

13. For Hauser bases with terminal bulky amide ligands, see: (a) $[HMDSMgBr]_2$:Yang, K. C.; Chang, C. C.; Huang, J. Y.; Lin, C. C.; Lee, G. H.; Wang, Y.; Chiang, M. Y. Synthesis, Characterization and Crystal Structures of Alkyl-,Alkynyl-,Alkoxo- and Halo-Magnesium Amides. *J. Organometalic. Chem.* **2002**, *648*, 176–187.; (b) $[HMDSMgCl]_2$: Bartlett, R. A.; Olmstead, M. M.; Power, P. P. Structural Characterization of the "Magnesylamine" $[(Et_2O)Mg(Cl)\{N(SiMe_3)_2\}]_2$ and the Two-Coordinate Magnesium Amide $Mg\{N(SiMePh_2)_2\}_2$. *Inorg. Chem.* **1994**, *33*, 4800–4803.; (d) $[(Bn_2N)_2Mg]_2$.2THF: Clegg, W.; Craig, F. J.; Henderson, K. W.; Kennedy, A. R.; Mulvey, R. E.; O'Neil, P. A.; Reed, D. Solid State Structures and Dynamic Solution Equilibria of Bis(Dibenzylamido)Magnesium Complexes: Aggregation Dependence on Stoichiometry and Denticity of Donor Solvent. *Inorg. Chem.* **1997**, *36*, 6238–6246.; (e) For monomeric $(HMDS)_2Mg$.2THF, see: Bradley, D. C.; Hursthouse, M. B.; Ibrahim, A. A.; Malik, K. M. A.; Motevalli, M.; Moseler, R.; Powell, H.; Runnacles, J. D.; Sullivan, A. C. Synthesis and chemistry of the bis (trimethylsilyl) amido bis-tetrahydrofuranates of the group 2 metals magnesium, calcium, strontium and barium. X-ray crystal structures of $Mg[N(SiMe_3)_2]_2 \cdot 2THF$ and related $Mn[N(SiMe_3)_2]_2 \cdot 2THF$. *Polyhedron*, **1990**, *9*, 2959–2964.

14. Organomagnesium amides are structurally characterized bases for challenging metallation

reactions: (a) Zhang, M.-X.; Eaton, P. E., BuMgN^{i}Pr$_2$: A New Base for Stoichiometric, Position-Selective Deprotonation of Cyclopropane Carboxamides and Other Weak CH Acids. *Angew. Chem., Int. Ed*. **2002***, 41*, 2169–2171.; (b) Conway, B.; Hevia, E.; Kennedy, A. R.; Mulvey, R. E.; Weatherstone, S., Synthesis and Characterisation of a Series of Alkylmagnesium Amide and Related Oxygen-Contaminated "Alkoxy" Compounds. *Dalton Trans.* **2005**, 1532–1544.; (c) Rappoport, Z.; Marek, I. The Chemistry of Organomagnesium Compounds; John Wiley & Sons Ltd., 2008.

15. For X-ray structures of organomagnesium amides, see: (a) *i*-PrMg(DIPA) and EtMg(TMP): Coates, G. E.; Ridley, D. Some Amino-Alkylmagnesium Complexes: Evidence for Three-Co-Ordinate Magnesium. *J. Chem. Soc. A. Inorganic, Phys. Theor. Chem.* **1967**, 56–59. (b) *s*-BuMg(HMDS) and *t*-BuMg(NR$_2$) - NR$_2$= DIPA, HMDS, TMP, Cy$_2$N, Bn$_2$N: see ref. 14b.; (c) *n*-BuMg(TMP): Hevia, E.; Kennedy, A. R.; Mulvey, R. E.; Weatherstone, S. Synthesis and Crystal Structure of [{^{n}BuMg(μ-TMP)}$_2$] and of a Homometallic Inverse Crown in Tetranuclear [{^{n}BuMg$_2$[μ-N(H)Dipp]$_2$(μ^3-OnBu)}$_2$]. *Angew. Chem., Int. Ed.* **2004**, *43*, 1709–1712.; (d) RCCMg(DIPA) - R= Ph, TMS: see ref. 13a.; (e) *t*-BuMg(NH*t*-Bu): Olmstead, M. M.; Grigsby, W. J.; Chacon, D. R.; Hascall, T.; Power, P. P. Reactions between Primary Amines and Magnesium or Zinc Dialkyls: Intermediates in Metal Imide Formation. *Inorganica Chim. Acta* **1996**, *251*, 273–284.; (f) MeMg(NHTIPS): Westerhausen, M.; Bollwein, T.; Makropoulos, N.; Piotrowski, H. Ligand Exchange Reaction between an Alkylzinc Primary Amide and a Dialkylmagnesium Compound: Crystal Structures of [(THF)MeMg-μ-N(H)Si(^{i}Pr)$_3$]$_2$ and (TMEDA)Mg[N(H)Si(*i*-Pr)$_3$]$_2$. *Inorg. Chem.* **2005**, *44*, 6439–6444.; (g) For a chelate organomagnesium amide: Henderson, K. W.; Mulvey, R. E.; Dorigo, A. E. Solvent induced disproportionation of alkyl(amido)magnesium species containing a (2-pyridyl)amido unit: synthetic, theoretical and NMR spectroscopic studies of bis(amido)magnesium compounds. *J. Organomet. Chem*. **1996**, 518, 139–146.; (h) For a review, see: Pinkus, A. G. Three-coordinate Magnesium: Coord. *Chem. Rev*. **1978**, 25, 173–197.

16. (a) Colas, K.; Martin-Montero, R.; Mendoza, A. Intermolecular Pummerer Coupling with Carbon Nucleophiles in Non-Electrophilic Media. *Angew. Chem., Int. Ed*. **2017**, *56*, 16042–16046.; (b) Colas, K.; Mendoza, A. Iterative Synthesis of Pluripotent Thioethers through Controlled Redox Fluctuation of Sulfur. *Synlett* **2018**, *29*, 1329–1333.

17. (a) Ruppenthal, S.; Brückner, R. Symmetric Diarylsulfoxides as Asymmetric Sulfinylating Reagents for Dialkylmagnesium Compounds. *J. Org. Chem.* **2015**, *80*, 897–910.; (b) Li-Yuan Bao, R.; Zhao, R.; Shi, L. Progress and Developments in the Turbo Grignard Reagent *i*-PrMgCl·LiCl: A Ten-Year Journey. *Chem. Commun.* **2015**, *51*, 6884–6900.; (c) Rauhut, C. B.;

Melzig, L.; Knochel, P. Meta- and Para-Difunctionalization of Arenes via a Sulfoxide-Magnesium Exchange Reaction. *Org. Lett.* **2008**, *10*, 3891–3894.; (d) Shi, L.; Chu, Y.; Knochel, P.; Mayr, H. Leaving Group Dependence of the Rates of Halogen-Magnesium Exchange Reactions. *Org. Lett.* **2012**, *14*, 2602–2605.; (e) Casoni, G.; Kucukdisli, M.; Fordham, J. M.; Burns, M.; Myers, E. L.; Aggarwal, V. K. α-Sulfinyl Benzoates as Precursors to Li and Mg Carbenoids for the Stereoselective Iterative Homologation of Boronic Esters. *J. Am. Chem. Soc.* **2017**, *139*, 11877–11886.; (f) Oae, S.; Uchida, Y. Ligand-Coupling Reactions of Hypervalent Species. *Acc. Chem. Res.* **1991**, *24*, 202–208.

18. Colas, K.; dos Santos, A. Catarina V. D.; Mendoza, A. *i*-$Pr_2NMgCl{\cdot}LiCl$ Enables the Synthesis of Ketones by Direct Addition of Grignard Reagents to Carboxylate Anions. *Org. Lett*. **2019**, *21*, 7908–7913.

19. For seminal work, see: (a) Eisch, J. J.; Galle, J. E. Organosilicon compounds with functional groups proximate to silicon. Feasible route to 1,2-epoxyalkyllithium reagents via the lithiation of epoxyethylsilanes. *J. Am. Chem. Soc.* **1976**, *98*, 4646-4648; for applications of β-oxyfunctionalized organolithiums, see: (b) Barluenga, J.; Yus, M.; Concellon, J. M.; Bernad, P. Direct and regioselective transformation of α-chlorocarbonyl compounds into alkenes and deuteroalkenes. *J. Org. Chem.* **1981**, *46*, 2721-2726.; (c) Barluenga, J.; Yus, M.; Concellón, J. M.; Bernad, P. One-pot and regioselective synthesis of alkenes and deuterioalkenes from α-chlorocarboxylic acid chlorides via a tandem addition of two different nucleophiles (Grignard reagents, hydride or deuteride) and further lithiation. *J. Org. Chem.* **1983**, *48*, 609-611.; (d) Barluenga, J.; Yus, M.; Concellón, J. M.; Bernad, P. Direct one-pot synthesis of terminal olefins and deuterio olefins from carboxylic acid chlorides. *J. Org. Chem.* **1983**, *48*, 3116-3118.; for a comprehensive review, see: (e) Nájera, C.; Yus, M. Functionalized Organolithium Compounds: New Synthetic Adventures. *Curr. Org. Chem.* **2003**, *7*, 867-926.

20. (a) García Ruano, J. L.; Alemán, J.; Cid, M. B.; Fernández-Ibáñez, M. Á.; Maestro, M. C.; Martín, M. R.; Martín-Castro, A. M. In Organosulfur Chemistry in Asymmetric Synthesis: Asymmetric Transformations Mediated by Sulfinyl Groups: Wiley-VCH; Weinheim, 2009. (b) Bur, S. K. In Comprehensive Organic Synthesis: Polonovski- and Pummerer-Type Reactions and the Nef Reaction: Elsevier Ltd., 2014. (c) Feldman, K. S. Modern Pummerer-Type Reactions. *Tetrahedron*. **2006**, *62*, 5003–5034. (d) Pulis, A. P.; Procter, D. J. C−H Coupling Reactions Directed by Sulfoxides: Teaching an Old Functional Group New Tricks. *Angew. Chem., Int. Ed.* **2016**, *55*, 9842–9860. (e) Bur, S. K.; Padwa, A. The Pummerer Reaction: Methodology and Strategy for the Synthesis of Heterocyclic Compounds. *Chem. Rev.* **2004**,

104, 2401–2432; for selected recent examples of Pummerer-based reactions, see: (f) Kaldre, D.; Maryasin, B.; Kaiser, D.; Gajsek, O.; González, L.; Maulide, N. An Asymmetric Redox Arylation: Chirality Transfer from Sulfur to Carbon through a Sulfonium [3,3]-Sigmatropic Rearrangement. *Angew. Chem., Int. Ed.* **2017**, *56*, 2212–2215; (g) Kaiser, D.; Veiros, L. F.; Maulide, N. Brønsted Acid-Mediated Hydrative Arylation of Unactivated Alkynes. *Chem. Eur. J.* **2016**, *22*, 4727–4732.; (h) Fernández-Salas, J. A.; Eberhart, A. J.; Procter, D. J. Metal-Free CH-CH-Type Cross-Coupling of Arenes and Alkynes Directed by a Multifunctional Sulfoxide Group. *J. Am. Chem. Soc.* **2016**, *138*, 790–793; (i) Peng, B.; Huang, X.; Xie, L.-G.; Maulide, N. A Brønsted Acid Catalyzed Redox Arylation. *Angew. Chem., Int. Ed.* **2014**, *53*, 8718–8721; (j) Eberhart, A. J.; Procter, D. J. Nucleophilic *Ortho* -Propargylation of Aryl Sulfoxides: An Interrupted Pummerer/Allenyl Thio-Claisen Rearrangement Sequence. *Angew. Chem., Int. Ed.* **2013**, *52*, 4008–4011; (k) Eberhart, A. J.; Imbriglio, J. E.; Procter, D. J. Nucleophilic Ortho Allylation of Aryl and Heteroaryl Sulfoxides. *Org. Lett.* **2011**, *13*, 5882–5885. (l) Yorimitsu, H. Cascades of Interrupted Pummerer Reaction-Sigmatropic Rearrangement. *Chem. Rec.* **2017**, *17*, 1156–1167. (m) Smith, L. H. S.; Coote, S. C.; Sneddon, H. E.; Procter, D. J. Beyond the Pummerer Reaction: Recent Developments in Thionium Ion Chemistry. *Angew. Chem., Int. Ed*, **2010**, *49*, 5832–5844.

21. Becke, A. D. Density functional Thermochemistry. III. The Role of Exact Exchange. *J. Chem. Phys*. **1993**, *98*, 5648−5652. (b) Lee, C.; Yang, W.; Parr, R. G. Development of the Colle-Salvetti Correlation-energy Formula into a Functional of the Electron Density. *Phys. Rev. B* **1988**, *37*, 785−789.

22. (a) Grimme, S.; Antony, J.; Ehrlich, S.; Krieg, H. A consistent and accurate Ab Initio parametrization of density functional dispersion correction (DFT-D) for the 94 elements H-Pu. *J. Chem. Phys*. **2010**, *132*, 154104. (b) Grimme, S.; Ehrlich, S.; Goerigk, L. Effect of the damping function in dispersion corrected density functional theory. *J. Comput. Chem.* **2011**, *32*, 1456–1465.

23. Liu, W.-B.; Schuman, D. P.; Yang, Y.-F.; Toutov, A. A.; Liang, Y.; Klare, H. F. T.; Nesnas, N.; Oestreich, M.; Blackmond, D. G.; Virgil, S. C.; et al. Potassium Tert-Butoxide-Catalyzed Dehydrogenative C−H Silylation of Heteroaromatics: A Combined Experimental and Computational Mechanistic Study. *J. Am. Chem. Soc* **2017**, *139*, 45.

24. (a) Ishimori, M.; Hagiwara, T.; Tsuruta, Teiji.; Kai, Y.; Yasuoka, N.; Kasai, N.; The structure and reactivity of $[Zn(OMe)_2(EtZnOMe)_6]$. *Bul. Chem. Soc. Jap.* **1976**, *49*, 1165-1166. (b) Ullrich, M.; Berger, R. J. F.; Jana, S.; Pape, T.; Fröhlich, R.; Mitzel, N. W. Organozinc Hydroxylamides: On the Bulk-Dependent Interplay of Nuclearity, Structure and Dynamics.

Dalt. Trans. **2011**, *40*, 1144–1157. (c) Petrus, R.; Sobota, P. Zinc Complexes Supported by Maltolato Ligands: Synthesis, Structure, Solution Behavior, and Application in Ring-Opening Polymerization of Lactides. *Organometallics.* **2012**, *31*, 4755–4762. (d) Athavale, S. V.; Simon, A.; Houk, K. N.; Denmark, S. E. Demystifying the Asymmetry-Amplifying, Autocatalytic Behaviour of the Soai Reaction through Structural, Mechanistic and Computational Studies. *Nat. Chem.* **2020**, *12*, 412–423.

25. Gaussian 09, Revision E.01, M. J. Frisch, G. W. Trucks, H. B. Schlegel, G. E. Scuseria, M. A. Robb, J. R. Cheeseman, G. Scalmani, V. Barone, B. Mennucci, G. A. Petersson, H. Nakatsuji, M. Caricato, X. Li, H. P. Hratchian, A. F. Izmaylov, J. Bloino, G. Zheng, J. L. Sonnenberg, M. Hada, M. Ehara, K. Toyota, R. Fukuda, J. Hasegawa, M. Ishida, T. Nakajima, Y. Honda, O. Kitao, H. Nakai, T. Vreven, J. A. Montgomery, Jr., J. E. Peralta, F. Ogliaro, M. Bearpark, J. J. Heyd, E. Brothers, K. N. Kudin, V. N. Staroverov, T. Keith, R. Kobayashi, J. Normand, K. Raghavachari, A. Rendell, J. C. Burant, S. S. Iyengar, J. Tomasi, M. Cossi, N. Rega, J. M. Millam, M. Klene, J. E. Knox, J. B. Cross, V. Bakken, C. Adamo, J. Jaramillo, R. Gomperts, R. E. Stratmann, O. Yazyev, A. J. Austin, R. Cammi, C. Pomelli, J. W. Ochterski, R. L. Martin, K. Morokuma, V. G. Zakrzewski, G. A. Voth, P. Salvador, J. J. Dannenberg, S. Dapprich, A. D. Daniels, O. Farkas, J. B. Foresman, J. V. Ortiz, J. Cioslowski, D. J. Fox, Gaussian, Inc., Wallingford CT, **2013**.

26. Marenich, A. V.; Cramer, C. J.; Truhlar, D. G. Universal solvation model based on solute electron density and a continuum model of the solvent defined by the bulk dielectric constant and atomic surface tensions. *J. Phys. Chem. B.* **2009**, *113*, 6378–6396.

10.1002/chem.202004164

TOC Graphics